Article

Membranes: a variety of energy landscapes for many transfer opportunities

Patrice Bacchin[1,*]

[1]   Laboratoire de Génie Chimique, Université de Toulouse, CNRS, INPT, UPS, Toulouse, France [2]   Affiliation
*   Correspondence: patrice.bacchin@univ-tlse3.fr; Tel.: +33-056-155-8163

Abstract: A membrane can be represented by an energy landscape that solutes or colloids must cross. A model accounting for the momentum and the mass balances on the membrane energy landscape establishes a new way of writing for the Darcy law. The counter pressure in the Darcy law is no longer written as the result of an osmotic pressure difference but rather as a function of colloid-membrane interactions. The ability of the model to describe the physics of the filtration is discussed in detail. This model is solved on a simplified energy landscape to derive analytical relationships that describe the selectivity and the counter pressure from ab-initio operating conditions. The model shows that the stiffness of the energy landscape has an impact on the process efficiency: a gradual increase in interactions (like with hourglass pore shape) can reduce the separation energetic cost. It allows the introduction of a new paradigm to increase membrane efficiency: the accumulation that is inherent to the separation must be distributed across the membrane. Asymmetric interactions thus lead to direction-dependent transfer properties and the membrane exhibits diode behavior. These new transfer opportunities are discussed.

Keywords: membrane transport ; osmosis ; interaction

1. Introduction

The transport of colloids across interfaces is still a scientific challenge meeting applications in many processes. Flow through semi-permeable membranes is a common process in living bodies (kidneys, membrane cells, etc.) and in industrial applications (filtration, desalting, etc.) [1]. Beyond these applications, the recent development of microfluidic experiments and the nano-scale engineering of interfaces have revived the question of the role played by colloid-surface interactions on transport across interfaces [2].

The transport of fluids across a membrane is classically determined with a modified Darcy law accounting for a counter osmotic pressure:

$$J = \frac{L_p}{\eta}(\Delta p - \sigma \Delta \Pi) \tag{1}$$

where J is the solvent flux through the membrane, L_p is the membrane permeability, η is the solvent viscosity, Δp is the transmembrane pressure and $\Delta \Pi$ is the transmembrane osmotic pressure. This writing derives from the semi-empirical formulation of Kedem and Katchalsky [3] that considers non-equilibrium thermodynamics with the assumption of linearity between the fluxes and the driving forces. This law introduces a Staverman coefficient, σ, that is difficult to interpret and still the subject of debate. Physically, Eq. 1 signifies that the intensity of the solvent flux is induced by a driving pressure which is the applied static pressure minus the osmotic pressure difference. It is therefore assumed that flows through the membrane are caused by the differences in chemical potentials occurring across the membrane.

43   Several points can be subject of discussion in this law. First, this law is integrated and does not
44   enable the accounting of a local concentration variation close to the interface. For this reason, this
45   relationship is often considered as a flow boundary condition in a filtration problem. Secondly, in
46   this approach the membrane is discontinuously treated as an infinitively thin membrane separating
47   two compartments: the membrane is therefore described with a partition coefficient that induces an
48   unrealistic concentration jump at the interface. For these reasons, such way of writing cannot help to
49   elucidate the "strange" transport mechanism of fluids at the nano-scale [4] (recently highlighted in
50   microfluidic experiment or with nanotube, aquaporin, etc.) and therefore to progress by designing
51   specific nanoscale molecule/pore interactions within artificial nano-pores in order to optimize the
52   transport [5].
53   A significant progress could be made by a better understanding of the roles played by colloid-
54   membrane interaction on these interfacial phenomena. This role has been qualitatively pointed out
55   since the earlier works on Brownian diffusion at the interface [6–8]. In 70's, several authors [9,10]
56   develop theoretical models to quantify the role of colloid-membrane interactions on the transport.
57   However, these models were not really developed and used by the membrane community. In these
58   last ten years, several authors pointed out again the important role played by solute or colloid-
59   membrane interactions on the transport through a membrane [11–14]. Recently, a two-fluid model
60   that introduces an energy landscape to account for colloid-membrane interactions has been proposed
61   [15]. Such a model describes the dynamics of osmotic flows with a set of continuous equations [16].
62   Additionally, this type of model can be helpful to explore how the membrane energy landscape can
63   change the transport efficiencies. The aim of this paper is to analyze the effect of the energy barrier
64   profile on the efficiency of the separation with membrane processes.

65   **2. Theoretical background and model development**

66   A transport model was recently established from the momentum balance for the fluid and the
67   colloid phase where the membrane is represented by an energy landscape [15]. The energy landscape
68   [17] maps the colloid-membrane interaction energy (related to Gibbs free energy that will be
69   expressed per unit of volume as a pressure, Π_i, referred to as interfacial pressure) for of all the spatial
70   positions of the colloids at the vicinity or inside the membrane. This map represents the overall
71   interactions between the colloids and the membrane interface (as for example DLVO and hydration
72   forces [18,19]). This map can also account for the energy required to change the colloid shape towards
73   a configuration that can make the passage through the pore possible (for example for deformable
74   particles or for extensible or unfolding proteins) [20]. The following sections of this paper will
75   establish the transport equations on an energy landscape (2.1), will present the formalism to describe
76   a membrane with an energy landscape (2.2) and will derive analytical relationships to express the
77   membrane selectivity and the counter pressure (2.3). A final section (2.4) will present a numerical
78   application of the model and its validation by comparing the results with the classical Kedem and
79   Katchalsky approach.

80   *2.1. Transport of colloids and fluid*

81   A two-fluid model based on an energy landscape enables the implementation of
82   colloid/membrane interactions in the fluid and colloids momentum and mass balances [15]. The two-
83   fluid (or mixture) model [21,22] allows the velocities of the colloid phase, $\boldsymbol{u}_c$ and of the fluid phase
84   to be defined. By addition, the velocity of the mixture phase, $\boldsymbol{u}_m$, can be determined (supplementary
85   information S1). From the application of the momentum balance [23], a set of equation that defines
86   these velocities can be written:

$$\frac{\phi}{V_p}\frac{u_m - u_c}{m(\phi)} - \nabla\Pi_{cc} - \phi\nabla\Pi_i = 0 \tag{2}$$

$$\frac{\eta_m}{k_p}\boldsymbol{u_m} + \nabla p + \phi\nabla\Pi_i = 0 \tag{3}$$

89   The momentum balance on the colloids phase (Eq. 2) establishes that the drag force acting on colloids
90   due to the slip velocity (first term) is counterbalanced by the osmotic pressure gradient (second term)
91   and the interfacial pressure gradient due to colloid/membrane interactions (third term). In the
92   momentum mixture balance (Eq. 3), the pressure drop - due to friction between the mixture and the
93   interface (first term) - is brought both by the fluid pressure gradient (second term) and the colloid-
94   membrane interaction (third term). This mathematical writing thus accounts for the interactions
95   between the different phases. Eq.3 signifies that the drag force acting on particles (**fluid-colloid** slip
96   velocity) is balanced by either **colloid-colloid** interactions (through the osmotic pressure, $\Pi_{cc}(\phi)$) or
97   by **colloid-membrane** interactions (through the interfacial pressure, $\Pi_i(x)$). Eq. 4 signifies that the
98   drag forces on the interface (**fluid-membrane** dissipation) are induced by the destocking of either the
99   fluid pressure (**fluid-fluid** interactions) or the **colloid-membrane** interactions.

100   In a more conventional form for membrane community, Eqs 2 and 3 express the mass flux, $j =$
101    $u_c \phi$, and the permeate flux, $J = u_m$:

$$j = J\phi - V_p m(\phi) \left(\frac{d\Pi_{cc}(\phi)}{dx} + \phi \frac{d\Pi_i(x)}{dx} \right) \tag{4}$$

$$J = -\frac{k_p(x)}{\eta} \left(\frac{dp(x)}{dx} + \phi \frac{d\Pi_i(x)}{dx} \right) \tag{5}$$

104   The writing of mass flux (Eq. 4) is similar to the conventional one: the mass flux results from the
105   interplay between an advective term, a diffusive term (linked to the collective diffusion accounting
106   for Brownian diffusion and colloid-colloid interaction via the gradient in osmotic pressure, $\frac{d\Pi_{cc}(\phi)}{dx}$)
107   and a migration term induced by colloid-membrane interactions (relative to the gradient of interfacial
108   pressure, $\phi \frac{d\Pi_i(x)}{dx}$). The coupling of these three terms helps to describe the main mechanisms that
109   occur during separations:

110   •   the coupling of convective and diffusive –entropic contribution- fluxes describes the polarization
111   concentration [24,25]
112   •   the coupling of convective and diffusive – contribution induced by colloid-colloid interaction -
113   fluxes describes the colloid flux paradox [26] and the existence a critical flux [27–29] for
114   homogeneous liquid-solid transition [30,31]
115   •   the coupling of convective flux and migration induced by colloid-membrane interactions
116   describes the heterogeneous critical flux phenomena [32,33]
117   •   the coupling of diffusive flux and migration induced by colloid-membrane interaction describes
118   the Boltzmann exclusion that is due to the colloid-membrane interaction [23]

119   However, a strong difference with conventional approaches appears in the expression of the
120   permeate flux (Eq. 5). The driving pressure is expressed as the combination of the applied static
121   pressure with the interfacial pressure due to colloid-membrane interaction, $\phi \frac{d\Pi_i(x)}{dx}$. The colloid
122   membrane interactions here play the role of a forcing term on the momentum equations of the fluid
123   flow, similarly to the Force Coupling Method used to describe multi-phase flows [34–36]. This
124   expression, based on a mechanical approach, presents significant differences with the classical
125   thermodynamic approach (Eq. 1) but is close to the Kedem and Katchalsky equations solved through
126   a potential-energy profile [20]. It should be noted that, in the limit of $j = J\phi$ or $u_m = u_c$ that
127   corresponds to negligible colloid-fluid drag force, the colloid membrane interaction are equal to the
128   gradient in osmotic pressure, $\phi \frac{d\Pi_i(x)}{dx} = -\frac{d\Pi_{cc}(\phi)}{dx}$. Under this assumption, the integration of Eq. 5
129   thus leads to Eq. 1. The main discrepancies occurring for others conditions will be discussed in detail
130   throughout the paper.

131   To determine the membrane transport, the set of equation (Eqs. 4 and 5) must be solved in the x
132   direction, perpendicular to the membrane surface, i.e. all along the polarization and the membrane
133   layers. The interfacial pressure variation, $\Pi_i(x)$, defines an energy landscape that represents the
134   colloid-membrane interactions which in turn control the membrane transport through the term
135    $\phi \frac{d\Pi_i(x)}{dx}$. This mechanical description is close to the thermodynamical model developed from a Kedem
136   and Katchalsky approach through a potential energy profile [9].

137   *2.2. Membranes as an energy landscape*

138   The membrane is represented by an energy map that defines the energy required to pass though
139   the membrane. The energy landscape can represent different separation pathways (Fig. 1) with the
140   possibility to account for patchy interactions. In landscape diversity, an infinitely thin and totally
141   retentive membrane is represented by an energy landscape being a Dirac delta function (the limit of
142   the normal distribution plotted in Fig. 1a) ; such a "perfect" landscape may represent a graphene
143   sheet.   In order to account for the transport inside the membrane thickness, the membrane can be
144   represented as a pulse of interfacial pressure (Fig. 1b). In this case, the increase in interfacial pressure
145   on both membrane side represent the partition induced by the presence of the membrane. This model
146   is then close to the one used by modeling approaches considering partitions at both side of an internal
147   pore where a coupling between convection and diffusion takes place [37]. But the energy landscape
148   can also describe less classical separation pathways, which can result from a nanoscale mosaic of
149   attractive and repulsive interactions. New opportunities are offered by nanofluidic systems to create
150   and investigate more complex interaction pathways that can bio-mimick biological membranes.
151   Asymmetric exclusion can be accounted for (Fig. 1c) to describe nanofluidic osmotic diodes [38]. The
152   interaction pathway can also exhibit internal energy wells (Fig. 1d) which can depict either double-
153   skin membranes, or, the presence of macro-pores inside the membranes. The stiffness of the
154   interaction pathway can also vary to represent, for example, membranes with a porosity gradient or
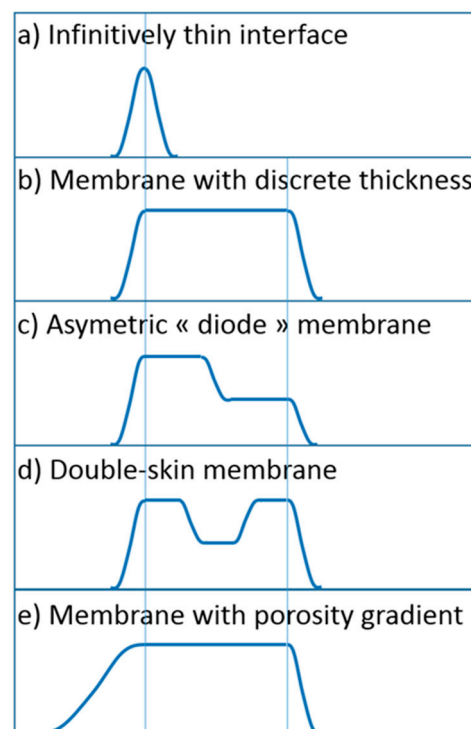155   hourglass pore shape (Fig. 1e).

156
157   **Figure 1.** Energy landscape representation of membrane diversity.
158
159   In this paper, the energy map for the membrane will be modeled in its simplest form in order to
160   analyze the essential ingredients of the model. The membrane is defined by two exclusion layers
161   (where a constant interfacial gradient takes place) bordering a zone with a constant interfacial
162   pressure (the gradient is zero and does not induce any forces in the momentum balances).   This case
163   can represent the energy landscape plotted in fig. 1b and 1e. The main parameters of the energy map
164   (Fig. 2) are the maximum value reached in the membrane, $\Pi_{i\,max}$ (that can be expressed in a non-
165   dimensional way, $Ex = \frac{V_p \Pi_{i\,max}}{kT}$) and the length of the ramp, δ_{EX}. In the case of an infinitesimally
166   thin membrane (demonstration in supplementary information S2), the exclusion number can be
167   linked to a partition coefficient, K, translating the Boltzmann exclusion induced by the energy map,
168    $K = e^{-Ex}$ [23]. The model will be applied through a series of composite layers (Fig. 2) that represent

169   the boundary layer thickness where concentration polarization occurs, the exclusion layer at the
170   membrane entrance, the membrane core thickness, the exclusion at the membrane outlet and the
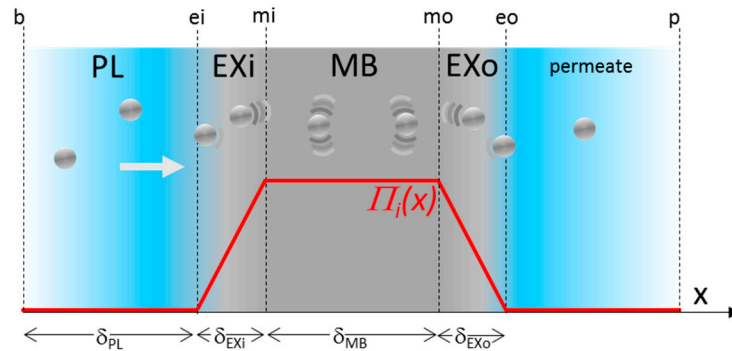171   permeate bulk.

172
173   **Figure 2.** The energy landscape representation of the interfacial pressure profile, Π_i,   along the
174   membrane thickness, x. The profile distinguishes the concentration polarization layer PL, the
175   inlet exclusion layer EXi, the membrane core thickness, MB, and the outlet exclusion layer,
176   EXo. The subscripts used for the value of the variables on these borders are b (bulk), ei (inlet
177   exclusion), mi (membrane inlet), mo (membrane outlet), eo (exclusion outlet) and p (permeate).
178
179

180   When applying the model (Eqs. 4-5) in these composite layers, the basis of physics are well
181   translated. In the polarization layer, the model describes the equivalence between drag force and the
182   gradient in osmotic pressure as already discussed by Wijmans et al. (1985) and   Elimelech and
183   Bhattacharjee (1998) for polarization concentration. As stated by Eq. 3, the pressure drop, ∇p, is zero
184   in the concentration polarization where there is no gradient in interfacial pressure, $\nabla \Pi_i = 0$.
185   Furthermore, in the absence of drag force (i.e. at equilibrium, $u_m = u_c$ in Eq. 2), the equation set
186   matches the description of the equilibrium between the static pressure and the osmotic pressure (Eq.
187   2 and 3 leads to $\nabla p = \nabla \Pi_{cc}$).

188   *2.2. Modelling the transmission and the counter pressure through the membrane*

189   At a steady state and if considering a linear variation of interfacial pressure in the exclusion
190   layers (Fig. 2), the application of the model enables the determination of analytical solutions. At a
191   steady state, the mass flux, j, and the permeate flux, J, are constant through the membrane. The
192   expression of the mass continuity (Eq. 4) in the composite layers determines the colloid concentration
193   profile through the membrane (supplementary information S3). By assuming the continuity of the
194   concentration through the composite layers, the ratio between the permeate concentration and the
195   feed concentration (i.e. the colloid transmission, Tr) can be determined (supplementary information
196   S4):

197
$$Tr = \frac{\phi_p}{\phi_b} = \frac{1}{1 + Ex\left(\frac{(e^{-(Pe_{EXo}+Ex)}-1)e^{-Pe_{MB}-Pe_{PL}-Pe_{EXi}+Ex}}{Pe_{EXo}+Ex} + \frac{(1-e^{-Pe_{EXi}+Ex})e^{-Pe_{PL}}}{Pe_{EXi}-Ex}\right)} \tag{6}$$

198   where Péclet numbers, $Pe = \frac{J\delta}{D}$, are defined for each layers (with the subscript PL, Exi, MB and Exo)
199   and, Ex, is the exclusion number defined in the previous section.
200   The permeate flow through the membrane, J, can be classically defined with a counter pressure,
201   CP, describing the osmosis flow. When Eq. 5 is integrated, the counter pressure can be expressed as
202   the integration of the interfacial force acting on all the particles in the exclusion layers $\int \phi d\Pi_i$:

203
$$J = \frac{L_p}{\eta}(\Delta P - CP) = \frac{L_p}{\mu}\left(\Delta P - \int \phi d\Pi_i\right) \tag{7}$$

204   The counter pressure can then be analytically calculated from the energy map, Π_i, and the
205   volume fraction profile, ϕ, determined previously. In the end (the calculation details are given in the

206 supplementary information S5), the counter pressure can be linked to osmotic pressures between the
207 composite layers (Eq. 8) or to the operating conditions (Eq. 9) :

$$CP = \Pi_{ei} - \Pi_{eo} + \Pi_{mo} - \Pi_{mi} + \frac{Pe_{EXi}}{Pe_{EXi} - Ex}\left(\Pi_{mi} - \Pi_{ei} + \Pi_p Ex\right) + \frac{Pe_{EXo}}{Pe_{EXo} + Ex}\left(\Pi_{eo} - \Pi_{mo} - \Pi_p Ex\right) \quad (8)$$

$$CP = Tr\frac{\Pi_b Ex^2}{AB}\left(\frac{B}{A}(e^{-A} - 1) + \frac{A}{B}(e^{-B} - 1) + A + B - (e^{-A} - 1)(e^{-B} - 1)e^{-Pe_{MB}}\right) \quad (9)$$

210 where $A = Pe_{EXi} - Ex$ and $B = Pe_{EXo} + Ex$. This last equation is particularly interesting as it
211 permits the counter pressure to be computed from ab-initio parameters. In contrast, the usual
212 calculation (Eq. 1) requires the knowledge of the difference of the osmotic pressure through the
213 membrane and the Staverman coefficient.

214 *2.4. Model application and validation*

215 To illustrate the ability of the model to describe membrane separation, calculations are now
216 shown. Calculations are performed for conditions where the exclusion layers are small (1/10)
217 compared to the others boundary layers: $Pe_{EXo} = Pe_{EXi} = 0.1Pe_{MB} = 0.1Pe_{PL} = 0.1Pe$. The value of
218 the partition coefficient is $e^{-Ex} = K = 0.1$. The transmission and the counter pressure determined
219 with the analytical model (Eqs. 6 and 9) are provided in Fig. 3 and 4 as a function of the Péclet
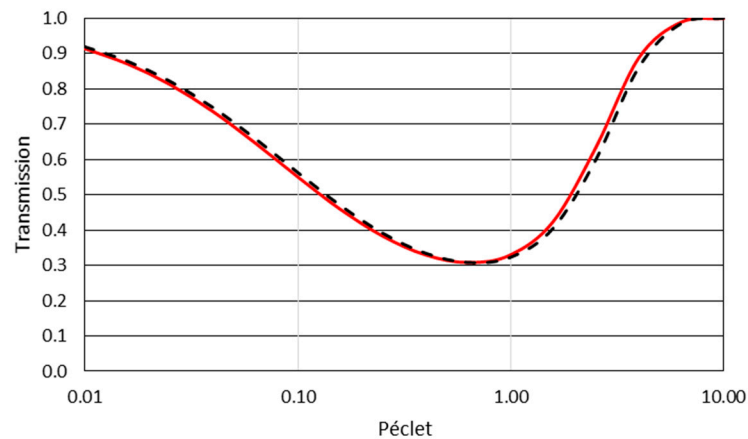220 numbers, Pe (defined as $Pe = Pe_{MB} = Pe_{PL}$).

221

222 **Figure 3.** Modelling of the transmission during a filtration for different Peclet number, $Pe = Pe_{MB} =$
223 Pe_{PL}. The model (full red line) is compared to the classical transmission model of Opong and Zydney
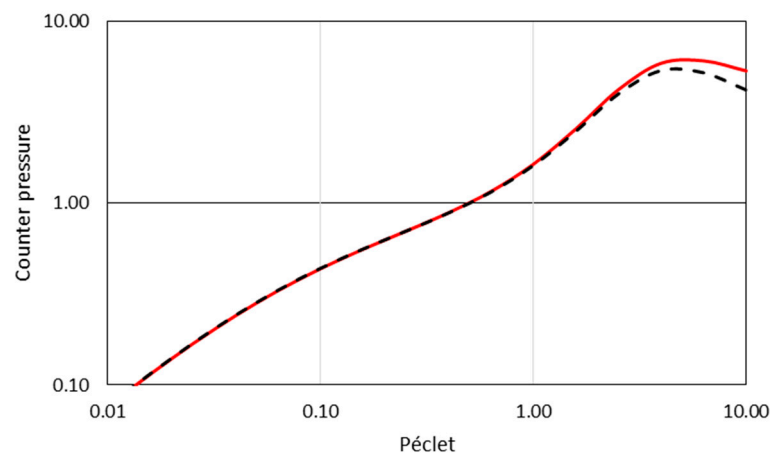224 [37].

225

226 **Figure 4.** Modelling of the counter pressure during a filtration for different Peclet number,Pe= Pe_{MB}
227 = Pe_{PL}. The model (full red line) is compared to the Kedem Katchalsky approach (dashed line) with
228 a Staverman coefficient, $\sigma = (1 - K)$.

229   It can be seen that the model for transmission (Eq. 6) provides results (Fig. 3) that are close to the
230 classical relationship developed for membrane filtration [37,41] or for electrokinetic salt rejection [42].
231 The convergence of the model to the cases of an infinitesimally thin membrane is demonstrated in S4
232 of the supplementary information. Fig. 4 plots the values of the counter pressure as a function of the
233 Pe numbers and compares the model to the classical approach, considering the osmotic pressure
234 difference weighted with the Staverman coefficient. To operate this comparison, the Staverman
235 coefficient [43] is defined as $\sigma = (1 - K)$ where K is the partition coefficient. Indeed, it can be
236 demonstrated (detail in SI 7), after several simplification and model assumptions (for an
237 infinitesimally thin membrane and for an osmotic pressure of colloids following the Van't Hoff law),
238 that the counter pressure given by the model is converging toward:

239
$$CP = (1 - K)(\Pi_m - \Pi_b) \tag{10}$$

240   This expression can also be seen as the contribution of $\Pi_{ei} - \Pi_{eo} + \Pi_{mo} - \Pi_{mi}$ in Eq. 8. Eq. 9 is
241 therefore coherent with the frequent writing of the Staverman coefficient (Eq. 1) as a reflection
242 coefficient accounting for the leakage of a membrane (σ ranging from 0 for a completely non-
243 retentive membrane to 1 for a membrane impermeable to the solute). The model therefore proposes
244 a demonstration and analytical writing for the Staverman coefficient that is still subject to different
245 interpretations of the Kedem and Katchaslky equations [44].

246   However, it must be noted, for the highest Péclet number (where conditions are highly
247 irreversible and far from near-equilibrium assumptions), that there is a gap between the model and
248 the Kedem Katchaslky Staverman approach, and the gap is amplified as the Péclet number increases
249 (Fig. 4). These differences are due to the drag force that occurs in the exclusion layers. Indeed, the
250 counter pressure results from the combination of an osmotic pressure difference and drag force (SI5):

251
$$J \quad = \frac{L_p}{\mu} \left(\Delta p_f \ - (1 - K)(\Pi_m - \Pi_b) - \int_{Exi+Exo} \frac{\phi}{V_p} F_{drag} dx \right) \tag{11}$$

252   Eq. 11 can be seen as an extension of the Kedem and Katchaslky approach which accounts for
253 the drag forces acting on arrested colloids. The drag force term is a frictional contribution that
254 describes the resistance to the flow induced by the arrested (but still dispersed) colloids in the
255 exclusion layers. Such a resistance may extend into a deposit flow resistance in the presence of a
256 consolidated deposit (not taken into account in this paper). The drag force contribution is also
257 represented by the last two terms in Eq. 8. This gap is becoming increasingly significant as the Peclet
258 number increases (Fig. 2b) or when the thickness of the exclusion layers becomes thinner, as
259 discussed in the following section.

260 **3. Impact of energy landscape stiffness**

261   In this section, the effect of the stiffness of the energy landscape on the membrane separation
262 efficiencies is investigated. To do this, different energy landscape profiles are considered as sketched
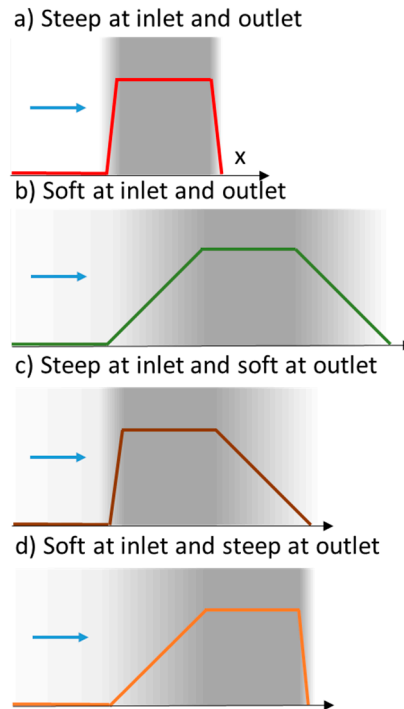263 in Fig. 5.

Figure 5. Energy landscapes considered for the analysis of the impact of the interaction stiffness. The steeper interactions occurs in thickness layers that are 1/10 of the membrane thickness. The softer interaction increases progressively in a thickness equal to the membrane thickness. For all cases, the thickness of the boundary layer is kept constant and equal to the membrane thickness.

In section 3.1, the effect of the interaction stiffness on transmission is analyzed. Such effect can lead to an asymmetric transmission of the solute, discussed in section 3.2. The model is used to analyze experimental results of the asymmetric transmission of DNA plasmid through membranes. The stiffness of colloid-membrane interactions has also important consequences on the counter pressure and thus on the energetics cost of the separation that are discussed in section 3.3. Towards the end (section 3.4), these phenomena lead us to consider a paradigm shift to improve membrane efficiency: the accumulation at the membrane should be distributed along the exclusion layers of the membrane.

3.1. Impacts of colloid-membrane stiffness on colloid transmission

The model enables the investigation of the effect of the energy landscape profile on transmission (Eq. 6). To illustrate this effect, transmission and counter pressure were calculated for softer interaction ramps where the layers thickness for exclusion are in the same range as the membrane and the polarization layer thicknesses (Fig. 5b). In these conditions, the Péclet numbers are all equal, $Pe_{EXo} = Pe_{EXi} = Pe_{MB} = Pe_{PL}$, whereas for steep ramp (Fig. 5a and results in section 2.4), $Pe_{EXo} = Pe_{EXi} = 0.1Pe_{MB} = 0.1Pe_{PL} = 0.1Pe$. Fig. 6 plots the transmission as a function of the Péclet number for these energy landscapes (Fig. 5). These results are compared to the relationship obtained when a partition coefficient depict the membrane exclusion (i.e. an infinitely thin exclusion layer –or infinitely steep interaction ramp-).
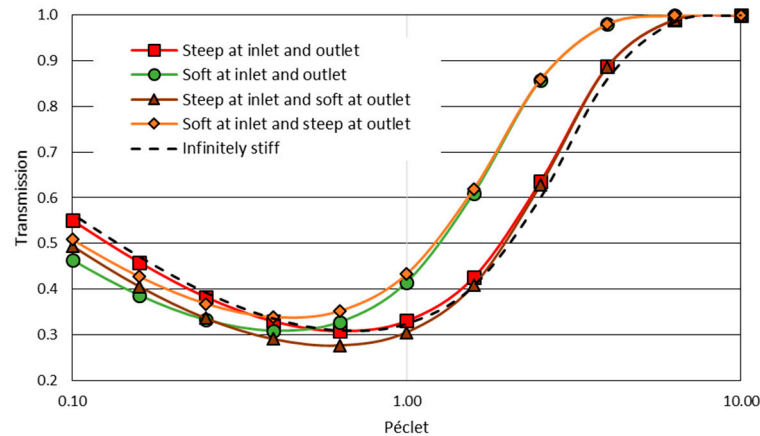
287

Figure 6. The effect of the exclusion ramp stiffness on the transmission

289   For Péclet values greater than one, a softer interaction ramp stiffness leads to a shift in
290   transmission towards smaller Péclet numbers. Thus, a similar transmission can be reached for smaller
291   Péclet values (the colloids "climb" the membrane energy barrier more easily). In this Péclet range,
292   the outlet ramp does not play an important role: the transmission is controlled by the stiffness of the
293   interaction at the inlet. For Péclet values less than one (where diffusion plays a significant role in the
294   transport), transmission is controlled by the total length of the membrane and the exclusion layers :
295   an increase in the total length of the membrane(due to thicker exclusion layers) leads to a decrease in
296   transmission of colloids.

297   *3.2. Asymetric transmission through a membrane*

298   The shift in transmission described by the model in the Fig. 6 has been observed in filtration
299   experiments carried out in two different directions [45]:

300   • with the flow directed from the bulk to the skin layer of the membrane (the interaction occurs
301   abruptly at the pore entrance) –referred to as forward filtration and corresponding to Fig. 5c-
302   • with the flow directed through the open pores in the substructure before the skin (the interaction
303   with the pore wall take place progressively) –referred to as reverse filtration and corresponding
304   to Fig. 5d-.
305   The experimental transmission of plasmid DNA obtained by Li et al. [45] in forward and reverse
306   filtration are represented by symbols in Fig. 7. The results demonstrate that the transmission of the
307   protein is facilitated when the filtration is performed in the reverse direction (Fig. 5d). The model (Eq.
308   6) has been used to interpret this data. The parameters of the model have been defined to have a good
309   fit between modeling and experimental data as follows:

310   • the forward filtration (through the skin layer supported on the macroporous support Fig. 5c)   is
311   represented with a thin exclusion layer at the inlet and a thick exclusion layer at the outlet,
312   Pe_{EXi}=0.1 Pe, Pe_{EXo}=5 Pe , Pe_{PL}=Pe_M=Pe
313   • the reverse filtration (through the macroporous layer first, Fig. 5d)   is represented   with a thick
314   exclusion layer at the inlet and a thin exclusion layer at the outlet, Pe_{EXi} =5 Pe, Pe_{EXo} =0.1 Pe ,
315   Pe_{PL}=Pe_M =Pe (thus corresponding to the reversal of the previous case).

316   For the fitting, the exclusion number is taken at 4.6 that corresponds, for infinitely thin
317   membrane, to a partition coefficient of 0.01. The transmission experiments are well represented by
318   the model (lines in Fig. 7). Furthermore, the fitting parameters are related to the physical conditions
319   of the experiments: the Péclet number for the transport in the macroporous layer (Pe_{EXo} in forward
320   and Pe_{EXi} in reverse direction) is 5 times higher than the one in the membrane. This proportionality
321   coefficient is in the range of the ratio of the length of the macroporous layer ($\simeq$ 10 micrometers) and
322   the length of the membrane skin layer ($\simeq$ 1 micrometer).

323   The enhanced transmission for the filtration in the reverse direction can thus be explained by
324   the fact that the energy landscape is more progressive. The softer interaction ramp can be the
325   consequence of the progressive spatial restrictions when filtering through the macroporous part of
326   the membrane. The protein-membrane interaction are therefore progressively increasing. These
327   interactions with walls can also lead to a change in the plasmid DNA conformation (as a plasmid
328   extension) that can also in turn soften the energy landscape (as initially discussed in [45]).
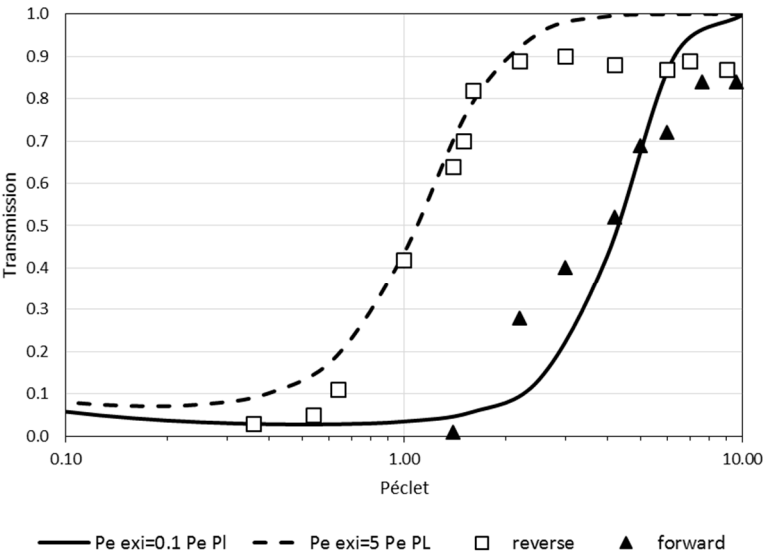

329

330   **Figure 7.** Protein transmission as a function of the Péclet number. The data is extracted from the paper
331   of Li et al. 2015 for plasmid filtration through a membrane in the forward direction –from the skin
332   layer to the macroporous layer- (full triangle) and in the reverse direction –from microporous to the
333   skin layer- (open square). The lines represent the results obtained with the model. The full line is
334   obtained for a thin exclusion layer at the inlet and a thick exclusion layer at the outlet (Pe_{Exi}=0.1 Pe,
335   Pe_{EXo}=5 Pe , Pe_{PL}=Pe_M=Pe) thus representing the filtration through a skin layer supported on a
336   macroporous support. The dashed line represents the results of the model for a thick exclusion layer
337   at the inlet and a thin exclusion layer at the outlet (Pe_{Exi}=5 Pe, Pe_{EXo}=0.1 Pe , Pe_{PL}=Pe_M=Pe)
338   corresponding to a case where the filtration is performed in the reverse direction.

339   This non-symmetric membrane transmission displays a diode behavior by exhibiting varying
340   resistance to the flow of protein according to the direction of use. Such behavior has been discussed
341   for nano-channels that have an asymmetry of surface charge [38] or during organic solvent
342   nanofiltration on membrane having an asymmetrical surface treatment [46]. Better knowledge of
343   such phenomena could help to develop new membrane design (with a porosity gradient for example)
344   which could improve transfer efficiency and could also help to understand the asymmetric
345   transmission observed with asymmetric biological cell membranes [47].

346   A membrane diode behavior can also open the possibility of a new mode of operation. If the
347   transmission depends on the flow direction, the pulsation of the flow through the membrane should
348   lead to separation without having an overall net flux across the membrane. Simple calculations,
349   taking into account a succession of steady state transmissions with a pulsed square flow, show the
350   possibility of separation after several flow pulses (supplementary information S6). Such a mode of
351   operation could find an interest in achieving the separation of very small volume.

352

353

354   *3.3. Softer colloid-membrane interaction ramp reduces the separation energy cost Asymetric transmission*
355   *through a membrane*

356   Softer interactions also lead to a decrease in the counter pressure (Fig. 8) when the Péclet number
357   is larger than one. For the same Péclet number, the counter pressure is lower when the interactions
358   occur in a progressive (or softer) way.
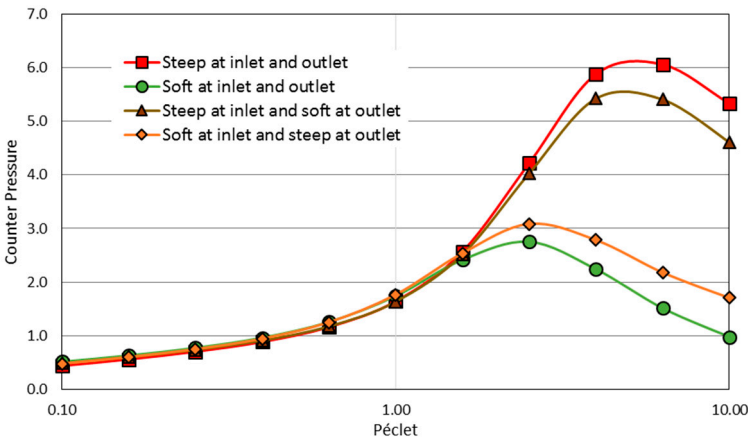

359

360   **Figure 8.** The effect of an exclusion ramp stiffness on the counter pressure

361   However, it is difficult to fully interpret these results as the transmission is simultaneously
362   varying with the Péclet number (as previously discussed with Fig.6). Thus, table 1 completes this
363   data with values of counter pressure obtained for a same selectivity (i.e. for a same separation
364   achievement). A same separation (a same transmission) can be achieved for 34% smaller Péclet
365   number in the case of soft interaction ramps. As a result, the counter pressure is significantly reduced
366   (-40 % when working with a 0.6 transmission or -55% for a 0.9 transmission).

367   **Table 1.** Counter pressure, CP, values obtained for a same transmission, Tr, and for different
368   conditions in the exclusion ramp stiffness. The counter pressure is compared to the difference of
369   osmotic pressure, $\Delta\Pi$.

	Tr	Pe	$V_p\Delta\Pi/kT$	CP/$\Delta\Pi$	CP (Pa)
Steep ramps	0.6	2.36	4.24 10^{-3}	0.95	3.96
Soft ramps	0.6	1.56 (-34 %)	1.90 10^{-3}	1.28	2.39 (-40 %)
Steep ramps	0.9	4.11	6.09 10^{-3}	0.99	5.95
Soft ramps	0.9	2.79 (-34 %)	1.63 10^{-3}	1.69	2.70 (-55 %)

370

371   The counter pressure also represents the minimal energy in Joules required to produce 1 m^3 of
372   permeate (without accounting for additional solvent frictions inside the membrane). It is therefore
373   interesting to plot the energy required to produce a permeate volume as a function of the process
374   selectivity, *1-Tr*. Fig. 9 thus represents the consumption (that should be decreased) as a function of
375   the selectivity (that should be increased). Moreover, to be economically sustainable, a separation
376   process must achieve a productivity that is defined by the Péclet number (the values are displayed in
377   text boxes in Fig. 9) that represents the flux intensity through the membrane.
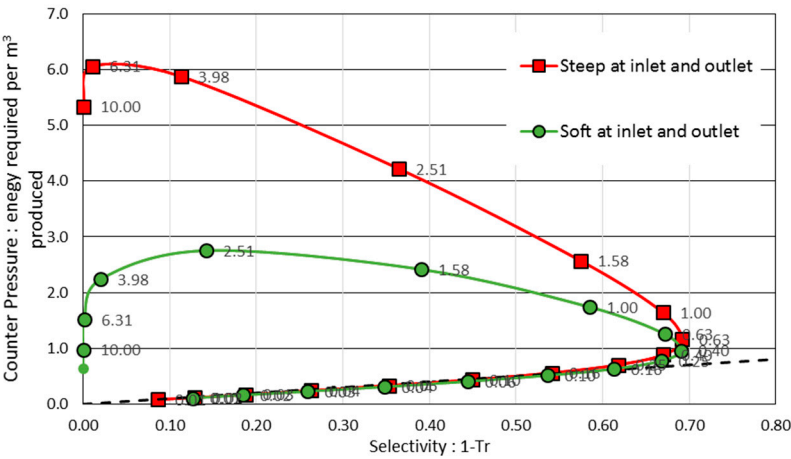
379 **Figure 9**. The benefit of a softer exclusion ramp on the separation efficiency (x axis) and energy costs
380 required for the separation (y axis). Text boxes located close to the symbols give the Péclet value that
381 indicates the productivity.

382 For very low productivity (*Pe* value less than 1), the energy required for passing through the
383 membrane is close to the bisector (dashed line) for which the counter pressure is equal to the
384 concentration difference. However, when Péclet values are greater than 1 the energy required for the
385 separation becomes significantly different according to the interactions conditions. This is mainly
386 because of the polarization concentration and the drag forces in the exclusion layer (last term in Eq.
387 10) that dissipate more energy in these far from equilibrium conditions. For a same selectivity, the
388 energy required for the transfer is less when the membrane interaction slope is softer mainly because
389 of the reduction of these drag forces. Such condition corresponds to a more sustainable way to operate
390 the separation. This could explain why hourglass shapes found in biological membrane transport
391 channels can improve the transfer efficiency [5].

392 *3.4. A new paradigm: the accumulation should be distributed*

393 These results must help to show the membrane separation from a different point of view. The
394 solute or the colloids transmissions through a membrane result from a potential barrier to overcome.
395 The energy to overcome the barrier comes from the drag force (the permeate flux) that is transmitted
396 on all the accumulated particles (the drag force must be multiplied by the number of accumulated
397 layers or by the accumulated volume). Colloid transmission (controlling membrane selectivity) and
398 colloid accumulation (controlling membrane productivity) are therefore fully linked. The colloid
399 transmission is the consequence of the accumulation that allows providing enough energy to the
400 colloids located close to the membrane to overcome the energy barrier and thus to pass through the
401 membrane. The transmission of a colloid through the membrane results from the transmission of
402 energy (due to drag force) through force chains in the network of accumulated colloids. But in usual
403 membrane approaches everything is done to limit the accumulation. From this work, a change of
404 paradigm can be considered. If considering that transmission needs some accumulation in order to
405 take place, the accumulation is then a necessity to ensure transmission. But, if the accumulation
406 occurs over a greater distance, a specific accumulated volume (controlling the transmission) can be
407 reached without implying high concentrations (Fig. 10). The accumulation is distributed over a larger
408 exclusion volume. As a consequence, for the same accumulated volume, the maximum concentration
409 at the pore entrance is less and the counter pressure is decreased. Such configuration leads to a
410 significant decrease in the energy cost for the separation. The main aim of the membrane user should
411 be to distribute the accumulation, not to decrease the accumulation. A soft ramp in the
412 colloid/membrane interaction is, for example, a way to distribute the accumulation and to perform
413 filtration with a lower energy cost. Researchers [45] have experimentally demonstrated that such
414 configuration could reduce fouling during protein filtration. The model can thus explain the gain due
415 to pore hourglass shape, frequently existing in biological membranes.

416   Contrary to these conclusions, it must be noted that, classically, the design of membrane pores
417   presents a sharp discontinuity in order to reject the accumulation outside the membrane. Indeed, the
418   use of hourglass shape should be carefully considered and this new paradigm cannot be extrapolated
419   to all the systems. This shape can represent an advantage, as previously discussed in this paper, only
420   if the solute-wall or the colloid-wall interactions are highly repulsive to prevent the adhesion of the
421   particles to the walls. For the opposite conditions, when this adhesion can occur, the hourglass shape
422   can favors the clogging. It has been experimentally shown that a convergent flow at a microchannel
423   bottleneck favor clogging by colloids [48]. Therefore, the hourglass shape should be combined with
424   repulsive interactions (for example patchy interactions like with zwitterionic groups) avoiding the
425   adhesion of the solute or the colloids to the wall. These theoretical findings could help to design
426   ultrafiltration, nanofiltration or reverse osmosis membranes with a gradient of porosity (or free
427   volume) in the skin layers and could help to elucidate the "strange" transport mechanism of fluids at
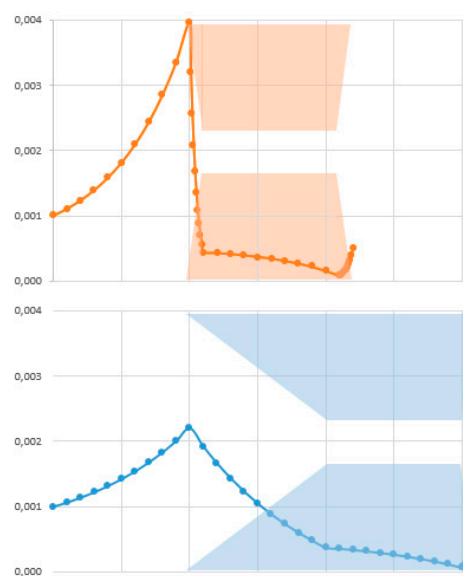428   the nanoscale [4].

429

430   **Figure 10.** Concentration profiles for a) steep interaction ramps (Fig. 5a) and b) soft interaction ramps
431   (Fig. 5d). The Péclet values are 1.93 and 1.22 for a) and b) respectively. For both cases, the transmission
432   is 0.5 and the exclusion number is 2.3. The soft interaction ramp leads to the distribution of the
433   accumulated mass all along the interacting membrane. This hourglass shape for the interacting
434   membrane leads a reduction in the maximum volume fraction, thus reducing the counter pressure
435   (the counter pressure are 3.19 and 2.08 Pa for a) and b) respectively). The efficiency of the transfer is
436   therefore higher in the case of soft interaction profiles.

4. Conclusions

438   A model, based on a two-fluid approach, has been solved in an energy landscape to account for
439   the colloid/membrane interactions. Colloid transmission and the counter pressure can be analytically
440   determined from ab-initio operating parameters. The model provides the theoretical origin of the
441   empirical writing of the Darcy law with the effective pressure given by the gap to the equilibrium,
442    $\Delta P - \sigma \Delta \Pi$. The Staverman coefficient, σ, is also theoretically linked to the partition coefficient of the
443   membrane and a gap to the Staverman approach due to drag forces is evidenced in far-from
444   equilibrium conditions. The ability of the model to describe the transport in an energy landscape is
445   illustrated by the investigation of the effect of a ramp of interaction. These results show that the
446   presence of progressive interactions increases the efficiency of the transport and decreases the
447   counter pressure. These results introduces a new paradigm: the accumulation should be distributed

448   along the membrane thickness, not decreased, to increase the separation efficiency. This work can
449   explain the results that show that filtration in a reverse direction (through the macroporous support)
450   can be more efficient than in a forward direction (through the skin). It gives a possible explanation
451   for the effect of the hourglass shape in membrane pore channels and for the membrane diode
452   behavior. It opens up interesting potentialities for the optimization of the membrane porosity design
453   and for the study of dynamic transport in pores with a nanoscale interaction mosaic, as for biological
454   membranes.

455   **Supplementary Materials:** The following are available online at www.mdpi.com/link, S1: Development and
456   main assumptions in the model, S2: Energy map model and Boltzmann exclusion, S3: Integration along the
457   membrane composite layers, S4: Relationships for the transmission, S5: Relationships for the counter pressure,
458   S6: Possibilities of separation with pulsed flow through asymmetric membranes

461

462   ## References

463   1.   Shannon, M. A.; Bohn, P. W.; Elimelech, M.; Georgiadis, J. G.; Mariñas, B. J.; Mayes, A. M. Science and
464   technology for water purification in the coming decades. *Nature* **2008**, *452*, 301–310,
465   doi:10.1038/nature06599.
466   2.   Bocquet, L.; Barrat, J.-L. Flow boundary conditions from nano- to micro-scales. *Soft Matter* **2007**, *3*, 685–693,
467   doi:10.1039/B616490K.
468   3.   Kedem, O.; Katchalsky, A. Thermodynamic analysis of the permeability of biological membranes to non-
469   electrolytes. *Biochim. Biophys. Acta* **1958**, *27*, 229–246, doi:10.1016/0006-3002(58)90330-5.
470   4.   Bocquet, L.; Charlaix, E. Nanofluidics, from bulk to interfaces. *Chem. Soc. Rev.* **2010**, *39*, 1073–1095,
471   doi:10.1039/B909366B.
472   5.   Gravelle, S.; Joly, L.; Detcheverry, F.; Ybert, C.; Cottin-Bizonne, C.; Bocquet, L. Optimizing water
473   permeability through the hourglass shape of aquaporins. *Proc. Natl. Acad. Sci.* **2013**, *110*, 16367–16372,
474   doi:10.1073/pnas.1306447110.
475   6.   Fermi, E. *Thermodynamics*; Dover publication.; 1936;
476   7.   van't Hoff, J. H. The role of osmotic pressure in the analogy between solutions and gases. *J. Membr. Sci.*
477   **1995**, *100*, 39–44, doi:10.1016/0376-7388(94)00232-N.
478   8.   Einstein, A. Investigations on the theory of the Brownian movement. *Ann Phys.* **1905**.
479   9.   Manning, G. S. Binary Diffusion and Bulk Flow through a Potential-Energy Profile: A Kinetic Basis for the
480   Thermodynamic Equations of Flow through Membranes. *J. Chem. Phys.* **1968**, *49*, 2668–2675,
481   doi:10.1063/1.1670468.
482   10.   Anderson, J. L.; Malone, D. M. Mechanism of Osmotic Flow in Porous Membranes. *Biophys. J.* **1974**, *14*, 957–
483   982, doi:10.1016/S0006-3495(74)85962-X.
484   11.   Cardoso, S. S. S.; Cartwright, J. H. E. Dynamics of osmosis in a porous medium. *R. Soc. Open Sci.* **2014**, *1*,
485   140352, doi:10.1098/rsos.140352.
486   12.   Lachish, U. Osmosis and thermodynamics. *Am. J. Phys.* **2007**, *75*, 997–998, doi:10.1119/1.2752822.
487   13.   Nelson, P. H. Osmosis and thermodynamics explained by solute blocking. *Eur. Biophys. J.* **2017**, *46*, 59–64,
488   doi:10.1007/s00249-016-1137-y.
489   14.   Kramer, E. M.; Myers, D. R. Osmosis is not driven by water dilution. *Trends Plant Sci.* **2013**, *18*, 195–197,
490   doi:10.1016/j.tplants.2012.12.001.
491   15.   Bacchin, P. An energy map model for colloid transport. *Chem. Eng. Sci.* **2017**, *158*, 208–215,
492   doi:10.1016/j.ces.2016.10.024.
493   16.   Bacchin, P. Colloid-interface interactions initiate osmotic flow dynamics. *Colloids Surf. Physicochem. Eng.*
494   *Asp.* **2017**, doi:10.1016/j.colsurfa.2017.08.034.
495   17.   Wales, D. *Energy Landscapes*; Cambridge University Press: Cambridge, 2004; ISBN 978-0-511-72172-4.
496   18.   Israelachvili, J.; Wennerström, H. Role of hydration and water structure in biological and colloidal
497   interactions. *Nature* **1996**, *379*, 219–225, doi:10.1038/379219a0.
498   19.   Verwey, E. J. W.; Overbeek, J. T. G. *Theory of the Stability of Lyophobic Colloids*; Courier Dover Publications,
499   1948; ISBN 978-0-486-40929-0.

20. Sastry, S.; Debenedetti, P. G.; Stillinger, F. H. Signatures of distinct dynamical regimes in the energy landscape of a glass-forming liquid. *Nature* **1998**, *393*, 554–557, doi:10.1038/31189.

21. Vollebregt, H. M.; van der Sman, R. G. M.; Boom, R. M. Suspension flow modelling in particle migration and microfiltration. *Soft Matter* **2010**, *6*, 6052, doi:10.1039/c0sm00217h.

22. Nott, P. R.; Guazzelli, E.; Pouliquen, O. The suspension balance model revisited. *Phys. Fluids 1994-Present* **2011**, *23*, 043304, doi:10.1063/1.3570921.

23. Bacchin, P. Dynamics of osmotic flows. *arXiv:1705.03248* **2017**.

24. ZYDNEY, A. L.; COLTON, C. K. A Concentration Polarization Model for the Filtrate Flux in Cross-Flow Microfiltration of Particulate Suspensions. *Chem. Eng. Commun.* **1986**, *47*, 1–21, doi:10.1080/00986448608911751.

25. Porter, M. C. Concentration Polarization with Membrane Ultrafiltration. *Prod. RD* **1972**, *11*, 234–248, doi:10.1021/i360043a002.

26. Cohen, R. .; Probstein, R. . Colloidal fouling of reverse osmosis membranes. *J. Colloid Interface Sci.* **1986**, *114*, 194–207, doi:10.1016/0021-9797(86)90252-3.

27. Jönsson, A.-S.; Jönsson, B. Ultrafiltration of Colloidal Dispersions—A Theoretical Model of the Concentration Polarization Phenomena. *J. Colloid Interface Sci.* **1996**, *180*, 504–518, doi:10.1006/jcis.1996.0331.

28. Bessiere, Y.; Abidine, N.; Bacchin, P. Low fouling conditions in dead-end filtration: Evidence for a critical filtered volume and interpretation using critical osmotic pressure. *J. Membr. Sci.* **2005**, *264*, 37–47, doi:10.1016/j.memsci.2005.04.018.

29. Bessiere, Y.; Fletcher, D. F.; Bacchin, P. Numerical simulation of colloid dead-end filtration: Effect of membrane characteristics and operating conditions on matter accumulation. *J. Membr. Sci.* **2008**, *313*, 52–59, doi:10.1016/j.memsci.2007.12.064.

30. Chen, V.; Fane, A. .; Madaeni, S.; Wenten, I. . Particle deposition during membrane filtration of colloids: transition between concentration polarization and cake formation. *J. Membr. Sci.* **1997**, *125*, 109–122, doi:10.1016/S0376-7388(96)00187-1.

31. Espinasse, B.; Bacchin, P.; Aimar, P. Filtration method characterizing the reversibility of colloidal fouling layers at a membrane surface: Analysis through critical flux and osmotic pressure. *J. Colloid Interface Sci.* **2008**, *320*, 483–490, doi:10.1016/j.jcis.2008.01.023.

32. Bacchin, P.; Aimar, P.; Sanchez, V. Model for colloidal fouling of membranes. *AIChE J.* **1995**, *41*, 368–376, doi:10.1002/aic.690410218.

33. Bacchin, P.; Marty, A.; Duru, P.; Meireles, M.; Aimar, P. Colloidal surface interactions and membrane fouling: Investigations at pore scale. *Adv. Colloid Interface Sci.* **2011**, *164*, 2–11, doi:10.1016/j.cis.2010.10.005.

34. Lomholt, S.; Maxey, M. R. Force-coupling method for particulate two-phase flow: Stokes flow. *J. Comput. Phys.* **2003**, *184*, 381–405, doi:10.1016/S0021-9991(02)00021-9.

35. Agbangla, G. C.; Climent, É.; Bacchin, P. Numerical investigation of channel blockage by flowing microparticles. *Comput. Fluids* **2014**, *94*, 69–83, doi:10.1016/j.compfluid.2014.01.018.

36. Agbangla, G. C.; Bacchin, P.; Climent, E. Collective dynamics of flowing colloids during pore clogging. *Soft Matter* **2014**, *10*, 6303–6315, doi:10.1039/C4SM00869C.